ADVANCED FUNCTIONAL MATERIALS
www.afm-journal.de

Spatially Controlled Delivery of siRNAs to Stem Cells in Implants Generated by Multi-Component Additive Manufacturing

Morten Østergaard Andersen, Dang Quang Svend Le, Muwan Chen, Jens Vinge Nygaard, Moustapha Kassem, Cody Bünger, and Jørgen Kjems**

Additive manufacturing is a promising technique in tissue engineering, as it enables truly individualized implants to be made to fit a particular defect. As previously shown, a feasible strategy to produce complex multicellular tissues is to deposit different small interfering RNA (siRNA) in porous implants that are subsequently sutured together. In this study, an additive manufacturing strategy to deposit carbohydrate hydrogels containing different siRNAs is applied into an implant, in a spatially controlled manner. When the obtained structures are seeded with mesenchymal stem (stromal) cells, the selected siRNAs are delivered to the cells and induces specific and localized gene silencing. Here, it is demonstrated how to replicate part of a patient's spinal cord from a computed tomography scan, using an additive manufacturing technique to produce an implant with compartmentalized siRNAs in the locations corresponding to distinct tissue. Hydrogel solutions loaded with different siRNA can be co-printed together with polycaprolactone that acts as rigid mechanical support to the hydrogel. This study demonstrates a new route for the production of 3D functionalized, individualized implants which may provide great clinical benefit.

1. Introduction

Tissue engineering (TE) is already revolutionizing medicine by providing autogenous transplantation organs including bladders[1] and tracheae,[2] but further developments are necessary before this potential can be realized for more complex organs or whole body parts.[3] One of the exciting prospects is individualized engineering of complex anatomically shaped tissues harboring multi lineage differentiated stem cells dictated by three-dimensional controlled cues. We have previously shown[4] that such implants can be assembled from porous polycaprolactone (PCL) building blocks containing two different siRNA and, upon seeding with stem cells and implantation into mice, induce the formation of pre-osteogenic and pre-adipocytic tissues in the predetermined locations. However, assembling implants from drug-loaded parts is a cumbersome procedure and is only feasible for certain tissue types wherein the different cell types are organized in macroscopic sections. To deal with more complex tissues, additive manufacturing (also known as rapid prototyping, 3D printing) is increasingly used in TE.[5]

Amongst 3D printing techniques, nozzle-based systems may be best suited;[6] however, there are several challenges with this technique that need to be addressed, including a limited range of biocompatible materials and the incorporation of cells and drugs.[6] Earlier approaches have typically focused on shaping an implant material into an anatomical correct shape and depositing different cell types in specific 3D geometries, in order to establish the cellular complexity of an organ. However, depositing drugs which induce differentiation of progenitor cells is another feasible route to generate bioactive scaffolds that has caught less attention. This approach has the advantage that it allows long term storage, which eases transportation and distribution, and enables the seeding of a single population of stem cells rather than multiple populations of terminally differentiated cells. Also, the applied population of stem cells can pass through their entire developmental program to become specialized cells in situ depositing vital extracellular matrix during the process.[7] Finally, compared to traditional scaffold

Dr. M. Ø. Andersen, Prof. J. Kjems
Department of Molecular Biology and Genetics
Aarhus University
C. F. Moellers Allé 3, Building 1130,
DK-8000 Aarhus C, Denmark
E-mail: morten.ostergaard.andersen@gmail.com; jk@mb.au.dk
Dr. M. Ø. Andersen, Dr. D. Q. S. Le, Dr. M. Chen, Dr. J. V. Nygaard, Prof. J. Kjems
Interdisciplinary Nanoscience Center (iNANO), Aarhus University
Gustav Wieds Vej 14, DK-8000 Aarhus C, Denmark
Dr. M. Ø. Andersen, Dr. D. Q. S. Le, Dr. M. Chen, Prof. C. Bünger
Orthopaedic Research Laboratory, Aarhus University Hospital
Nørrebrogade 44(1a), DK-8000 Aarhus C, Denmark
Dr. J. V. Nygaard
Department of Engineering, Aarhus University,
Finlandsgade 22, DK-8000 Aarhus C, Denmark
Prof. M. Kassem
Molecular Endocrinology Laboratory
Odense University Hospital
J. B. Winsløws Vej 25, DK-5000 Odense C, Denmark

DOI: 10.1002/adfm.201300832

manufacturing methods, additive manufacturing does not require the use of toxic organic solvents that may pose a health risk to the manufacturer and the patient.[8] The objective of this study was therefore to develop an approach by which a computed tomography (CT) scan could be used to direct the deposition of different drugs into specific volumes in 3D printed hydrogels, allowing them to program differentiation of subsequent seeded stem cells.

A number of different polymers have been applied as precursors to tissue engineering hydrogels, including various hydrocolloids of natural origin, which are hydrophilic polymers that generally are heavily hydroxylated. They can be derived from vegetable, animal, microbial, or synthetic sources and have been extensively studied and employed by the food industry as additives to manipulate texture, water binding, and emulsion stability of food items.[9] Such hydrocolloids are safe for oral ingestion and can readily be adapted for intestinal drug delivery.[10] Drug loaded hydrocolloid delivery devices can control the drug release rate into the intestinal lumen by limiting drug diffusion rate through the bulk polymer network. The use of vegetable derived hydrocolloids and gels for tissue engineering is more problematic, since the $\beta(1 \rightarrow 4)$-glycosidic bonds present in celluloses and most indigestible carbohydrate polymers are not readily degraded by human enzymes.[11] Also, the lack of receptor-recognizable groups on vegetable carbohydrate, along with lowered protein adsorption on highly hydrated, swollen surfaces, further decreases chances for cell attachment resulting in lower biocompatibility.[12] Vegetable hydrocolloids are, however, still widely used in tissue engineering where they often are used as non-toxic, non-immunogenic cell encapsulation materials. The seaweed-derived carbohydrate, sodium alginate, is widely used for its benign mode of forming hydrogels through ionotropic cross-linking with Ca^{2+}.[13,14] In the context of fused deposition modeling for scaffold fabrication, the use of hydrocolloids for generation of pseudoplastic properties is also highly important. In aqueous solution, hydrocolloid backbones have large gyration radii at rest, which immobilizes a comparable large volume of water. Under shear, the chains will curl up and lower the viscosity. Hydroxyethylcellulose (HEC) is a thermogelling carbohydrate[15] that behaves like a Bingham plastic. Such materials behave as solids at low stresses but flow as a viscous fluid at high stress. HEC enables the hydrogel to be extruded and then solidify during fused deposition modeling.

Several types of drugs exist that can be used to direct tissue development including protein growth factors, plasmid DNA, and viral vectors.[16–18] One important new class of molecules is the gene silencing non-coding RNAs (ncRNA) such as the synthetic small interfering RNA (siRNA) and the natural microRNA (miRNA) that can inhibit gene expression by RNA interference (RNAi).[19] When these RNAs are delivered as double stranded RNA to the cytoplasm, one of their strands is incorporated into the RISC complex, which it subsequently guides to specific mRNA(s) via base pairing, causing the mRNAs to be silenced by degradation, destabilization, or inhibition of translation. Tissue development can thus be controlled using siRNAs and miRNA by programming of the gene expression.[20] Compared to other molecules, synthetic siRNAs (or siRNA mimicking miRNA) have the distinct advantage that they all have the same size and charge, and differ only in the sequence of their constituent bases. Therefore, once a delivery system that induces gene silencing in stem cells has been developed, the same platform can be used as a generic approach to promote multi-linage stem differentiation of stem cells simply by targeting the siRNA to different genes.[21] Hence, scaffolds functionalized with RNAi active nucleic acids have become established as a key technology in recent tissue engineering strategies.[22–26] Here, we combine the versatility provided by RNAi with the spatial deposition of siRNAs using a multicomponent additive manufacturing technique, and prove the functionality based on a reporter system and potential applicability for individualized engineering of complex 3D tissues.

2. Results

An overview of the materials preparation, implant manufacturing, and cell seeding is shown in **Figure 1**. Initially, we formulated 18 different gel compositions (0%, 0.2%, and 0.4% hyaluronic acid; 1% and 2% alginate and 4%, 7%, and 11% HEC) to assess printability (promoted mainly by HEC), stability (promoted mainly by alginate crosslinking), as well as cell attachment and survival (promoted mainly by hyaluronic acid) during three weeks of human mesenchymal stem cells (hMSC) (green fluorescence protein, GFP^+) cell culture (data not shown). Formulations that contained little or no hyaluronic acid showed poor cell survival, formulations with 7% or 11% HEC were best for printing but displayed, together the 1% alginate samples, poor stability during cell culture. A mix containing 0.4% hyaluronic acid, 2% alginate, and 4% HEC was chosen being most optimal for cell attachment and a reasonable balance between printability and cell culture stability. Such constructs stayed stabile in normal complete minimum essential medium (MEM) and supported growth of healthy cells for 21 days in culture (Supporting Information, Figure 1).

Freeze drying can cause siRNA complexes to irreversibly aggregate and lose activity.[27] To determine whether the siRNA complexes used in this study can withstand freeze drying, lipofectamine2000/siRNA complexes were prepared, analyzed for size and surface charge before and after lyophilization and rehydration. Their hydrodynamic radius before lyophilization was 970 nm (±46 nm) and the zeta potential was −19.5 mV (±0.76 mV), after rehydration the hydrodynamic radius was 952 nm (±77 nm) and the zeta potential was −18.7 mV (±1.85 mV). Gels with and without Lipofectamine2000/siRNA complexes were formulated, lyophilized, and visualized using low-vacuum scanning electron microscopy (**Figure 2**). All implants displayed a highly porous structure with pore size adequate for cell infiltration during the loading procedure. The addition of siRNA complexes did not alter the implant microstructure as judged from the SEM pictures.

Dehydrated hydrogels with Cy5- or fluorescein amidite (FAM) labelled siRNA were rehydrated with 200 000 hMSCs (GFP^-) in complete MEM supplemented with 40 mM $CaCl_2$. After 24 h the cells were extracted, washed, and analyzed for fluorescence using flow cytometry (**Figure 3**a). Cells from the Cy5-siRNA loaded gels were 2.55 times more red fluorescent

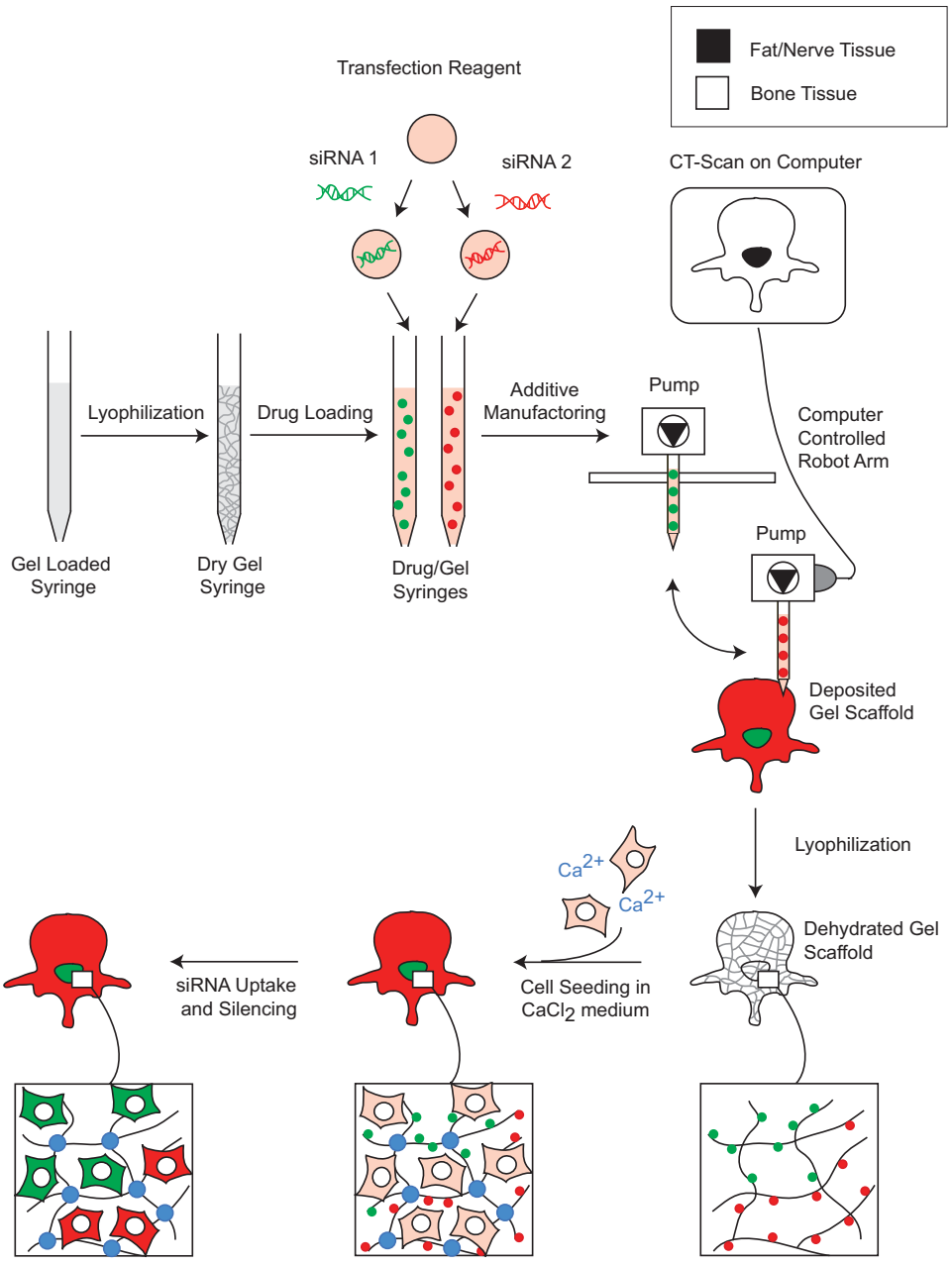

Figure 1. An overview of the implant manufacturing procedure used in the study.

than cells from FAM-siRNA loaded gels (significance: p = 0.000085; number of biological replicates: N = 5). Cells from the FAM-siRNA loaded gels were 1.12 times more green fluorescent than cells from Cy5-siRNA loaded gels; however, this increase was not statistically significant. When viewed as a histogram it can be seen that FAM-siRNA and Cy5-siRNA loaded gels gave rise to similar cell population distributions except that the entire cell population in the Cy5-siRNA loaded gels was shifted towards higher fluorescence, indicating that the transfection efficiency is close to 100% within the siRNA loaded gels (Figure 3c). The FAM-siRNA did not perform as well as the Cy5-siRNA (Figure 3b), most likely due to a higher background fluorescence signal from the gel at the shorter wavelengths. Lyophilized gels with or without Lipofectamine2000 formulated siRNA targeted against GFP or a mismatched negative control siRNA were seeded with 200 000 hMSCs (GFP^+ or GFP^-) in complete MEM supplemented with 40 mM $CaCl_2$. After 1 day, the medium was changed to fresh regular complete MEM. After a total of 72 h of incubation, the cells were extracted, washed, and analyzed by flow cytometry (Figure 3d). The inclusion of an siRNA targeted to GFP resulted in 46% and 43% silencing of GFP compared to no siRNA (p = 0.019, N = 3) or a mismatched siRNA (p = 0.020, N = 3), respectively, when adjusting for the auto fluorescence of GFP^- cells.

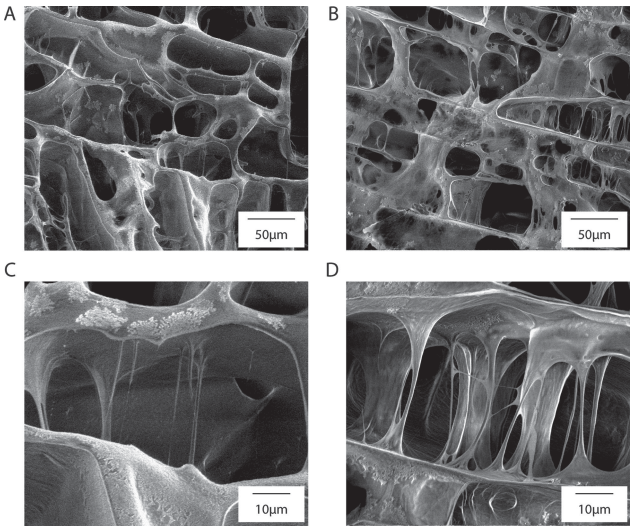

Figure 2. Scanning electron microscopy pictures of lyophilized hydrogels B,D) with and A,C) without lipofectamine2000/siRNA nanoparticles taken at A,B) 500× and C,D) 2000× magnification.

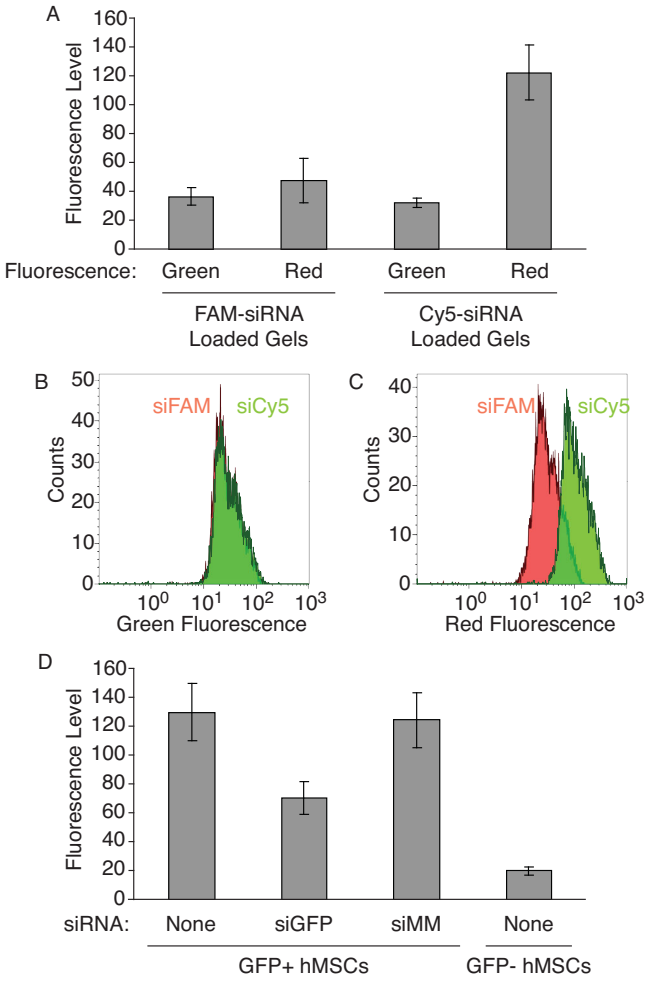

Figure 3. Flow cytometric analysis of hMSCs grown in hydrogels loaded with different siRNAs. A–C) Cells grown for 24 h in hydrogels loaded with Cy5- or FAM-labelled siRNA. D) Cells grown for 72 h in hydrogels loaded with GFP targeted (siGFP) or mismatched (siMM) siRNA.

Next, we turned to the printing of gels containing spatially deposited siRNAs. To conduct a proof of concept study, we used a CT section from a patient's spinal cord (**Figure 4**a) to define various regions as "dense" or "soft" tissue within a 3D model. In this model, the "soft" center represents the Canalis Spinalis and the "dense" sides the back of the vertebrae (Figure 4b). This was then used as a blueprint to direct the bioscaffolder to print a Cy5-labelled siRNA containing gel in the "soft" regions and a FAM-labelled siRNA containing gel to the "dense" regions (Figure 4c). The printed scaffolds (Figure 4d) were lyophilized and placed in 6-well plates with non-adherence wells. They were then seeded with 10^6 GFP^- hMSCs in 1 mL of complete MEM containing 40 mM $CaCl_2$. After 24 h in culture, the medium was aspirated and the gels were scanned for red and green fluorescence using a typhoon fluorescence scanner (Figure 4e). Red and green fluorescence corresponding to the "dense" and "soft" regions, respectively, in the original CT-scan were clearly detected. This shows that the siRNA only marginally diffuses between the "dense" and "soft" regions over the time of the experiment.

To ensure that the localized fluorescence is associated with the cells, we extracted the cells from the spinal plots using citrate and subjected them to flow cytometry (**Figure 5**). The cells extracted from the center (soft region) of the plot had 2.19 times more red fluorescence (Cy5-siRNA) compared to the cells from the outer part of the gel structure (hard region). Significantly ($p = 0.04$, $N = 6$), they also displayed 2.84 times more red (Cy5-siRNA) fluorescence than green fluorescence (FAM-siRNA) at the exposure levels used. In contrast, the red fluorescence was only 1.36 times higher in the outer part of the section, a difference which was not significant. The ratio of red fluorescence between cells from the center and outer part was significantly ($p = 0.03$, $N = 6$) higher than the similar ratio of green fluorescence. Histograms (Figure 5b–c) indicate that the cells from the FAM-siRNA loaded outer parts are homogenously shifted towards higher green fluorescence relative to the Cy5-siRNA loaded center part indicating close to 100% uptake efficiency. The cells from the center part, while displaying greater red fluorescence than the outer part, show a two-peaked population. This could be because of a lower uptake efficiency in this part or diffusion of the FAM-siRNA complexes from the outer part into the center part, but more likely it is a technical issue, as we may have transferred some of the outer section together with the center part when separating the two sections before flow cytometry (the center and outer parts are indistinguishable after cell culture). While gels based purely on cross-linked alginate and other carbohydrates may be strong enough to form the structural basis of soft tissues, the engineering of connective tissues necessitates a load-bearing component until the developing tissue has grown strong enough to bear the load on its own.[28] Towards this we evaluated whether we could co-print a PCL skeleton along with two gels containing either Cy5- or Cy3-labelled siRNA. To determine the degree of spatial restriction we printed the gels and PCL into a 4 × 4 checkered

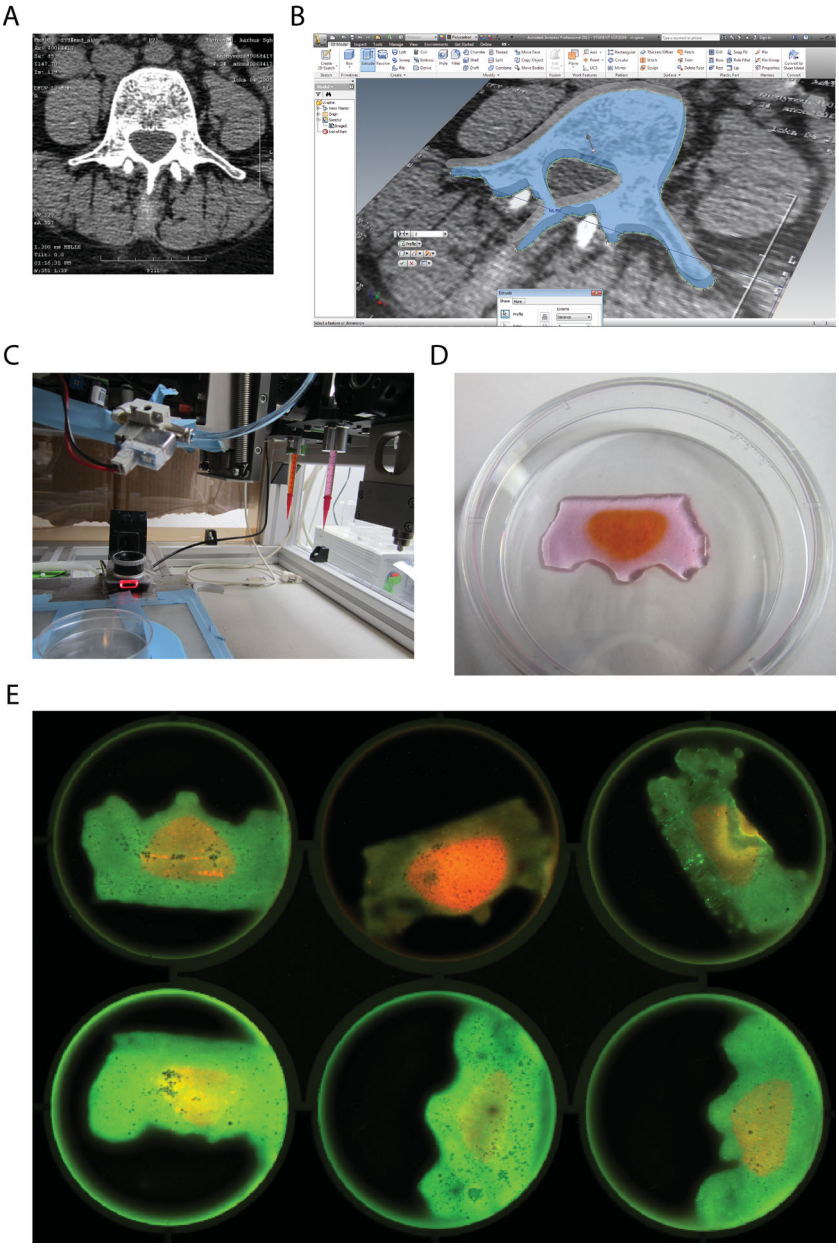

Figure 4. A) Vertebra geometry was reverse engineered from a CT scan and B) used to establish a multicomponent model of a patient's spine. C) The model was then printed to produce spinal implants containing D) two types of hydrogel containing either Cy5-labelled or FAM-labelled siRNA; E) these were lyophilized, seeded with cells and visualized after 24 hours incubation in medium using a typhoon fluorescence scanner. Red corresponds to the Cy5-siRNA signal, green to FAM-siRNA. The size of the implants is 1:1 to the patient CT-scan. The edges of some of the samples look rough as they are out of focus and the "tip" of the upper-left scaffold is folded under the rest of the structure as a result of the difficulties of getting the gels to lie flat and even on the bottom of the well given time constraints necessary to avoid drying and bleaching of the scaffolds.

pattern (**Figure 6**). Adding PCL fibers to the hydrogels greatly increased the mechanical strength and resulted in implants that were impossible to crush by hand. The implants were lyophilized and seeded with 10^6 GFP^+ hMSCs in 1 mL of complete MEM containing 40 mM $CaCl_2$. After 24 h in culture, the medium was aspirated and the gels were scanned for red and green fluorescence using a typhoon fluorescence scanner. Subsequently, fresh complete MEM without $CaCl_2$ was added and, after another 72 h, the implants were rescanned and visualized using fluorescence microscopy. The Cy3 and Cy5 fluorescence signals were highly localized after 1 day (Figure 6a,b) whereas the GFP signal from the cells is spread out evenly over the implant (Figure 6c). At day 4, the Cy3 and Cy5 fluorescence is still localized but less markedly than at day 1 (Figure 6d,e). At this point, the cells remained spread out evenly over the implant (Figure 6f); furthermore, the cells appeared healthy and were stretching out along the PCL fibers (Figure 6g), whereas only very few cells remained unattached in the gel.

To confirm that compartmentalization of the siRNAs translates into localized gene silencing, we printed a PCL based scaffold with a 4 × 4 checkered pattern of two alternating hydrogels, one with GFP targeting siRNA and one with mismatched siRNA. The lyophilized implant was seeded with 2 000 000 cells in complete MEM supplemented with 40 mM $CaCl_2$. After 24 h, the medium was changed to regular complete MEM and, after an additional 48 h, knockdown was quantified. Several attempts to quantify knockdown by flow cytometry failed as the cells attached too strongly to the PCL for detachment using citrate, ethylenediaminetetraacetic acid (EDTA), and trypsin, and quantitative polymerase chain reaction was hampered by the large quantity of PCL interfering with RNA isolation. Therefore, the implant was scanned for green fluorescence using a typhoon scanner and knockdown was estimated from the scan (**Figure 7**). It was evident that the cell derived GFP fluorescence signal was stronger on the PCL fibers than in the interspersed hydrogel (Figure 7a), confirming Figure 6g which showed that the cells prefer to grow on the PCL fibers rather than in the gel. Despite a smear of increased fluorescence at the corners and edges (which is caused by traces of liquid scattering light), quantification revealed that the green fluorescence signal was on average 49% lower in the squares containing GFP targeted siRNA (p = 0,041, N = 8). In Figure 3b auto-fluorescence from GFP^- hMSCs in the GFP channel was determined to be 16% of the total GFP fluorescence in the mismatch sample. Assuming a similar level of auto fluorescence, in this experiment, the real level of GFP silencing is 58% (Figure 7d), though this probably underestimates the silencing efficiency, as PCL, which was not present in Figure 3b, is autofluorescent.[4]

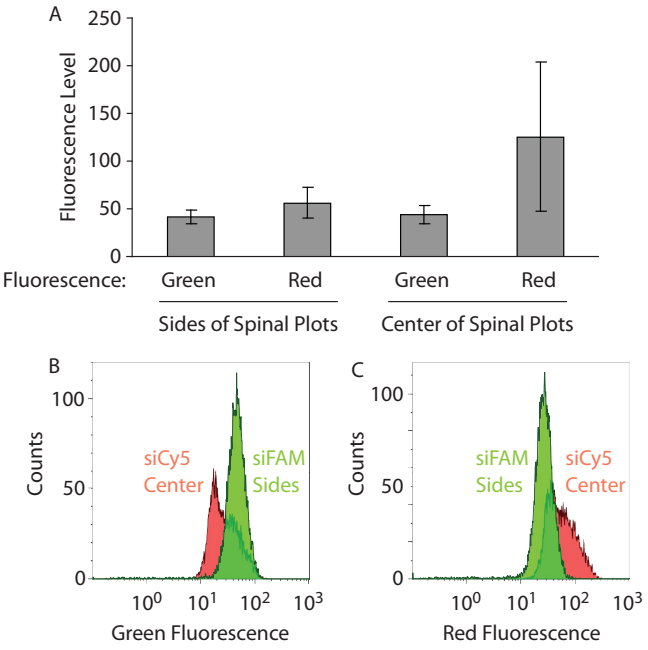

Figure 5. Flow cytometric analysis of cells extracted from spinal implants. Cells were harvested either from the center of spinal implants or from the outer part of the scaffold and analysed by flow cytometry measuring green (FAM) and red (Cy5) fluorescence.

3. Discussion

Drug and/or cell loaded hydrogels have been used widely for the engineering of various tissues. In this study, we developed a hydrogel for fused deposition modeling composed of three components: hyaluronic acid, alginate, and hydroxyethylcellulose that provide a gel with optimal cell biocompatibility, serum stability, and printability. To our knowledge, this is the first time these three components have been applied together in an implant. PCL and alginate have previously been co-printed to produce scaffolds where PCL provided mechanical strength.[29] We confirm that this is a viable approach to improve handling of the gels and their load bearing capacity, and that it can also be used when drug loaded hydrogels are printed. We also observed that the hMSC cells rapidly adhered to the hard PCL skeleton instead of being dispersed in the hydrogel, confirming a previous study that showed that endothelial cells prefer and actively migrate towards hard substrates.[30]

The most common mode of fused deposition modeling for tissue engineering uses biocompatible thermoplastic polymers such as polycaprolactone, polylactic acid, or polylactic-co-glycolic acid.[31–33] Thermoplastics exhibit viscous flow, while molten and can thus be easily deposited and solidify when cooled, which stabilizes the unfinished scaffold preventing it from collapsing and, at the same time, increasing the build height. Unfortunately, since the melting temperatures of all of these polymers have necessarily to be above body temperature, co-deposition of thermolabile drugs and proteins necessitates a hydrogel carrier.

Fabrication of rapid prototyped scaffolds using hydrogels has been done using alginate solutions, where the dispensing is done with simultaneous exposure to a cross-linking Ca^{2+} solution.[34,35] The simpler approach involves dispensing the solution into a plotting medium with carefully matched density and rheological properties.[36] The method of printing into a plotting medium can, however, be a disadvantage when working with drug loaded hydrogels, due to the risk of drug leaching during printing and removal of plotting medium. Furthermore, the plotting medium can inadvertently be incorporated into the hydrogel.

Adding a shear thinning viscosity modifier to the printing solution can, to some extent, obviate the need for a plotting medium, thereby simplifying the plotting setup. In our case, we added a small amount of the carbohydrate hydroxyethylcellulose to the gel. Dissolved HEC is clear, odorless, tasteless, nontoxic, resistant to biodegradation, and physiologically inert. HEC have high degrees of pseudo-plasticity, as well as high shear stability over long period.[16] At concentrations above approximately 2%, pure HEC solutions are highly viscoplastic showing some degrees of tensile and compressive strength.

Inclusion of HEC to the alginate/hyaluronic acid formulation made the already highly viscous and homogeneous solution behave as a Bingham plastic that could be steadily extruded through 25 gauge and even 27 gauge conical dispensing tips with no signs of syneresis. Pseudoplastic materials rapidly decrease in viscosity with increase in shear stress and pseudoplastic flow is present a physiological temperatures, which is important when choosing materials for constructing scaffolds containing temperature-sensitive components, that is, sensitive drugs or living cells. An additional advantage of the shear thinning properties is that, during extrusion, the majority of the volume passing through the conical tip is shielded from shear stress. This is a useful property for high throughput printing of living cells and drugs.

siRNAs and the natural miRNAs are promising drugs in tissue engineering because of their versatility.[20,21] For instance, siRNAs against BCL2L2 and TRIB2 have been applied to promote the formation of bone and adipose tissues present in the CT-scan.[4] While plasmid DNA has previously been printed successfully,[37] previous studies have shown that cells may be damaged by certain forms of printing.[38] A concern could be that printing the hydrogel together with 80 °C hot PCL (the approximate temperature of the PCL when it reaches the plate) and leaving it to air dry for one hour could destroy the siRNA and its activity. Our result shows that the silencing activity of the siRNA was preserved, indicating that the co-printing siRNA loaded hydrogel with melted PCL is a viable strategy. This, and the retention of their physical parameters upon lyophilization, also confirms our previous findings that some siRNA lipoplexes can be freeze dried without lyoprotectants.[27] Importantly, our lipoplexes did not induce any significant non-specific silencing, commonly seen in siRNA transfection experiments using these types of transfection reagents. Another important property of the transfection complexes is the size and charge that will influence mobility in the gel. Lipofectamine2000/DNA complexes have previously been shown to be ≈1 µm in diameter and negatively charged,[39] here, we show that, after lyophilization, the

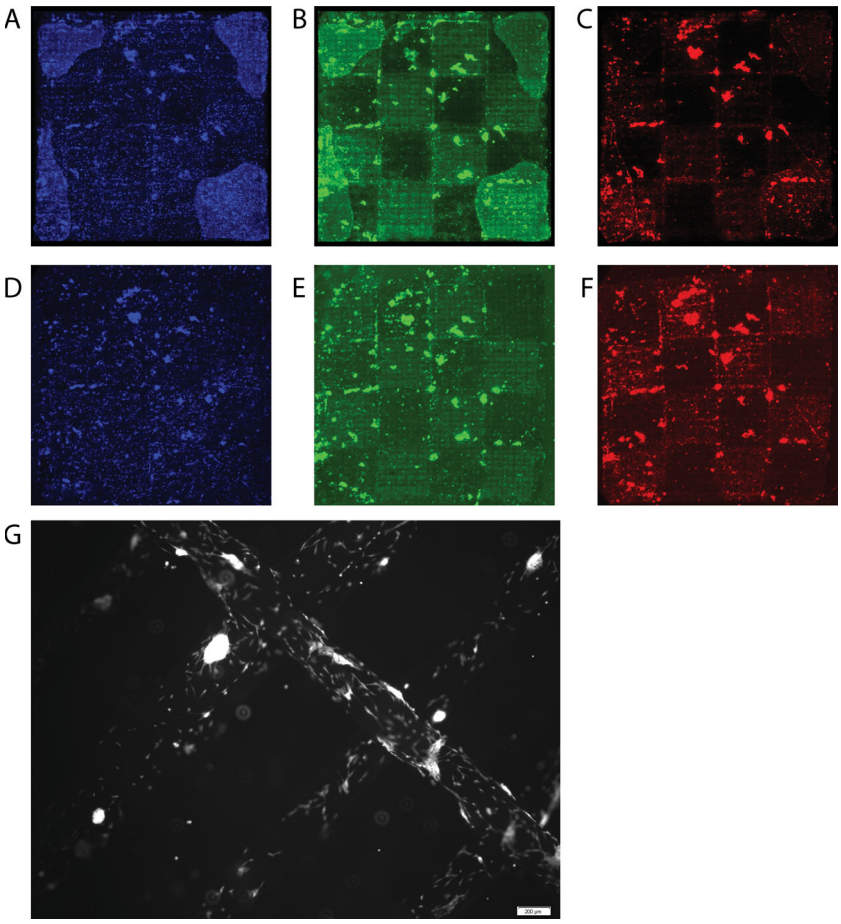

Figure 6. Visualization of checkered patterned implants consisting of two co-printed loaded hydrogels containing Cy3 and Cy5 labelled siRNA and a PCL fiber scaffold. The implants were seeded with hMSCs (GFP^+) and scanned at A–C) day 1 and D–G) day 4. The colors respond to the light of excitation: A,D,G) blue or white is GFP, B,E) green is Cy3, and C,F) red is Cy5.

transfection complexes used in this study rehydrated into negatively charged particles with diameters just below one micrometer. Presumably, these particles will not interact strongly with the negatively charged alginate and hyaluronic acid or neutral hydroxyethylcellulose polymers, but their relatively large size may help restrict them to the volumes wherein they are deposited. Alternatively, smaller RNA delivery particles may be used if they are positively charged, as electrostatic interaction may then compensate for less steric hindrance to limit diffusion. While this study focuses on RNA delivery, the technique we develop in this paper is not limited to this class of drugs and it could easily be modified to enable multi-component printing of other sensitive entities including DNA, protein growth factors or cells.

We demonstrate that it is feasible to print three-dimensional structures where different siRNAs, placed in predesignated locations, remain spatially restricted and active. Such a system enables individualized tissue engineering where patient scanning data is used directly to program the printing process of an implant with correct tissue types. Our cell-free printing approach has the advantage that the printed structures are dehydrated and, therefore, easier to store and distribute. The surgeon only has to seed stem cells which can be isolated within the operating room, eliminating the need for transportation and storage of stem cells between clinical procedures. Another advantage is that undifferentiated stem cells can be seeded and undergo differentiation into specialized cell types after reimplantation. During their differentiation, stem cells secrete a number of extracellular matrix proteins that are important for the fully differentiated tissue function, a feature not provided by terminally differentiated cells.[7] Although seeding of stem cells after printing worked well in our system, we expect that for larger scaffolds combining stem cell and drug printing will work more optimally, to insure better cell deposition in the interior of the scaffold.

Another exciting use for the technology is as a high throughput 3D screening platform for cellular cues. Determining the effect of various miRNAs alone or in combination with growth factors and/or small molecules in parallel may enable the determination of new drug cocktails and lead molecules relevant to the pharmaceutical industry. Such screening is typically carried out with transfected cell arrays,[40] which have the inherent drawbacks of being 2D. Firstly, we demonstrate a technique to print a 3D array with different drugs localized in predetermined volumes. Within each compartment, cells grow on a carbohydrate polymer support mimicking the actual extracellular environment experienced by the cell in vivo. Secondly, while we essentially kept our small 3D volumes in a 2D array due to limitations in our fluorescence scanning equipment, the technique could easily be used to print larger 3D boxes containing n^3 cubes with different drugs, where their induced phenotype could be assessed by confocal visualization. Such a system would offer a vast increase in the sizes of libraries that can be screened for cellular function.

4. Conclusion

The present study demonstrates that multiple hydrogels loaded with different drugs, in this case siRNA, can be deposited into a pre-programmed shape replicating a true tissue morphology using an automated additive manufacturing technique. When stem cells are seeded onto these structures, the siRNAs stay localized and are taken up by nearby cells wherein they induce sequence specific gene silencing. When using RNAs that induce stem cell differentiation, this technique may be used to create individualized tissues and organs composed of multiple cell types arranged internally to fit scanning data.

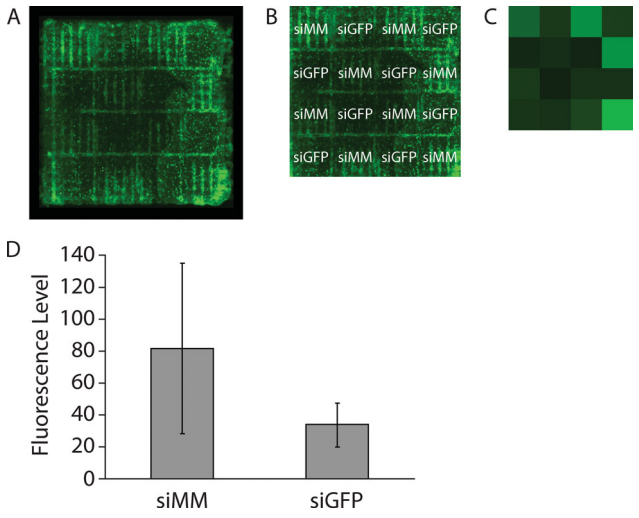

Figure 7. Visualization of checker patterned implants consisting of two co-printed loaded hydrogels containing GFP targeted or mismatched siRNA and a PCL fiber scaffold. A) The implants were seeded with hMSCs (GFP^+) and the implants were scanned at day 3 using a typhoon scanner. B) To quantify fluorescence levels, the scanning picture was cropped to and centered on the implant. C) A bilinear downsampling was then performed to 4 × 4 pixels representing the 4 × 4 siRNA squares. D) The color level (fluorescence value) of each pixel was thereafter quantified and each group averaged.

5. Experimental Section

Materials: Alginate powder and HEC powder was purchased from Sigma-Aldrich (Denmark). Research Grade 601K–850K Sodium Hyaluronate Powder was from LifeCore Inc. (FL). GFP-targeted, GFP-mismatched, FAM-labelled, Cy3-labelled and Cy5-labelled GFP-targeted siRNA were from Ribotask (Denmark). The sense sequences were: 5'-GACGUAAACGGCCACAAGUUCdTdT-3' (siGFP) and 5'-GACGUUAGACUGACAAGUUCdTdT-3' (siMM). Non-adherence plates (Costar) were from Corning (Netherlands). Lipofectamine2000 was from Invitrogen (USA).

Gel Production: Aqueous solutions were formulated containing 4% HEC, 2% alginate, and 0.5% hyaluronic acid by weight. The specific mixing ratio of hydrocolloids was determined by preliminary plotting and cell attachment studies. The solution was made by first dissolving alginate in water, then hyaluronic acid, lastly HEC, the latter forming a suspension at room temperature. The highly viscous, heterogeneous mixture was aspirated into 1 mL syringes, which were then sealed with syringe caps and heated to 100 °C in a water bath to dissolve the HEC. The syringes were then frozen and lyophilized at –20 °C. The dried gel formed a highly porous network inside the syringe which allowed fast and even rehydration with the transfection complex solution. This approach minimizes the occurrence of air bubbles inside the prepared gel, which is crucial in pneumatic dispensing. It furthermore addresses the desire to avoid shearing mixing of gel and particles.

Transfection Complex Formation & Incorporation: Lipofectamine2000 complexes were made by mixing 15 µL (1×) or 30 µL (2×) 20 µM siRNA with 500 µL MEM and 15 µL (1×) or 30 µL (2×) transfection reagent with 500 µL MEM; after 5 min, the solutions were combined and, after 20 min, 1 mL of the complexes were added to 1 mL of dried gel in a 1 mL syringe. The gel was left at room temperature until it had turned transparent (≈30 min) after which the gel was deposited into a polystyrene petri dish using a bioscaffolder (SYS+ENG GmbH, Germany) or by hand in non-adherence 24-well plates. The plates were frozen on dry ice and freeze dried until dry at –20 °C and 12 mTorr (at least 24 h). The dehydrated bioplotted structures were subsequently moved into 6-well non-adherence plates prior to cell loading. The 1× formulation was used for Figures 2,6,7, and the 2× formulation for Figures 3,4,5.

Dynamic Light Scattering and Zeta Potential Measurements: 1 mL of 1× Lipofectamine2000/siRNA particles were formulated and analyzed on a Zetasizer Nano ZS (Malvern Instruments Ltd, UK). The sample was then frozen on dry ice and freeze dried at –20 °C for 2 days at 12 mTorr in 1.5 mL tubes. After lyophilization, the complexes were resuspended in 1 mL ddH_2O and measured again. Z-Average size was used as the measure for hydrodynamic radius. All measurements were performed in triplicates.

Fused Deposition Modelling: Stereolithography (STL) files were made from a clinical, transverse CT image of a lumbar vertebra using Autodesk Inventor 2010 (Autodesk, CA). The final drawings were cropped at the vertebral body and the spinous and transversal processes, as the emphasis was on the interface between the spinal canal and the surrounding vertebra. The STL files were imported into PrimCAM (Primus Data, Germany) and printed at room temperature with a bioscaffolder using two separate pneumatic gel dispensers, each holding a 1 mL syringe with the plunger removed (Supporting Information, Video 1). The gels were extruded as 200 µm wide fibers from a 25 gauge tapered dispensing tip (EFD, RI). There were not notable indications of syneresis during the entire printing process. The center-to-center fiber spacing was set to 200 µm to create a solid gel. A total of 9 layers were deposited. The setup and gel deposition can be seen in Video 1, Supporting Information.

Scanning Electron Microscopy: Serum free MEM or Lipofectamine2000/siRNA complexes were incorporated into the gels. After freeze drying, the gels were glued onto aluminium stubs and imaged using scanning electron microscopy (SEM) with a NOVA nanoSEM 600 (FEI, OR) using a TLD detector, 5 kV voltage, and either 200× or 2000× magnification. Representative areas are shown.

Cell Culture and Seeding: Telomerase immortalized human mesenchymal stem cells were maintained at 37 °C and 5% CO_2 in MEM supplemented with 10% fetal bovine serum, 1% penicillin, and streptomycin solution (called complete MEM subsequently). Two populations were used, one with and one without an additional GFP expressing vector insert.[41,42] The GFP^- hMSCs were used between passage 35 and 45, whereas the GFP^+ hMSCs were used between passage 55 and 62. To load the gels with cells, a given number of cells were pelleted by centrifugation at 1500 rpm and resuspended in complete MEM adding 40 mM $CaCl_2$. The cell solution was then added to each dried scaffold in a volume corresponding to the pre-lyophilization volume of that scaffold. The gels wetted immediately and cross-linked due to the alginate. The gels were then incubated 24 h, after which 1 mL (24-well plate) or 4 mL (petri dish) of complete medium without $CaCl_2$ was added.

Flow Cytometry: To isolate the cells, each gel was washed with phosphate buffered saline (PBS); in the case of the spine plot, the sides and center were separated using a razor blade. The gels were transferred to 1.5 mL tubes and added 1 mL 50 mM sodium citrate. The tubes were turned for 20 min at 99 RPM to disperse the gels, if insufficiently dispersed additional pipette mixing using a p1000 pipette was used. After the gels were dissolved, the cells were pelleted by centrifugation at 1500 rpm for 5 min. The pellet was then resuspended in 1 mL 50 mM sodium citrate and analysed by flow cytometry immediately using either a Gallios or a FACScalibur flow cytometer. Forward and sidescatter was used to identify the cell population for which the mean green fluorescence was determined.

Fluorescence Scanning and Microscopy: The medium was aspirated from the wells, which were washed with warm PBS that was removed before the plate was transferred to a fluorescence scanner (Typhoon Trio, GE Healthcare). The plates were scanned for FAM/GFP, Cy3, and Cy5 fluorescence using the default settings; sensitivity was set to high and PMT to 500 (600 for Cy3), the resolution to 50 µm per pixel and the focus plane was set to +3 mm. The plates were scanned with the lid on to maintain sterility. After scanning (15–30 min) the plates were immediately returned to the incubator. Fluorescence microscopy was

performed using a fluorescence microscope (Olympus IX71 equipped with GFP filter, 10× objective and a mercury burner U-RFL-T as light source).

Statistics: All graphs show averages with standard deviation on the error bars. Two-tailed T-tests making no assumptions about equal variance were used to determine which groups were statistically significantly different. In the case of the spinal plots, where two types of cells were extracted from each implant (Figure 4), a two-tailed paired T-Test was used to test for differences. In all cases, a *p*-value below 0.05 was determined to be significant, the *N* given together each *p*-value is the number of biological replicates.

Supporting Information

Supporting Information is available from the Wiley Online Library or from the author.

Acknowledgements

The authors would like to thank Claus Bus and Rita Rosendahl Hansen for valuable technical assistance. This study is supported by grants from the Danish Strategic Research Council (Individualized Musculoskeletal Repair Network, Jr. nr. 09-063120), and Lundbeck Foundation Nanomedicine Center for Individualized Management of Tissue Damage and Regeneration (LUNA).

Received: March 7, 2013
Revised: April 23, 2013
Published online: June 3, 2013

[1] A. Atala, S. B. Bauer, S. Soker, J. J. Yoo, A. B. Retik, *Lancet* **2006**, *367*, 1241
[2] P. Macchiarini, P. Jungebluth, T. Go, M. A. Asnaghi, L. E. Rees, T. A. Cogan, A. Dodson, J. Martorell, S. Bellini, P. P. Parnigotto, S. C. Dickinson, A. P. Hollander, S. Mantero, M. T. Conconi, M. A. Birchall, *Lancet* **2008**, *372*, 2023.
[3] B. Derby, *Science* **2012**, *338*, 921.
[4] M. Ø. Andersen, J. V. Nygaard, J. S. Burns, M. K. Raarup, J. R. Nyengaard, C. Bünger, F. Besenbacher, K. A. Howard, M. Kassem, J. Kjems, *Mol. Ther.* **2010**, *18*, 2018.
[5] S. M. Peltola, F. P. W. Melchels, D. W. Grijpma, M. Kellomaki, *Ann. Med.* **2008**, *40*, 268.
[6] T. Billiet, M. Vandenhaute, J. Schelfhout, S. Van Vlierberghe, P. Dubruel, *Biomaterials* **2012**, *33*, 6020.
[7] J. E. Aubin, F. Liu, L. Malaval, A. K. Gupta, *Bone* **1995**, *17*, 77S.
[8] E. Sachlos, J. T. Czernuszka, *Eur. Cell. Mater.* **2003**, *5*, 29.
[9] H. Sahin, F. Ozdemir, *Food Hydrocolloids* **2004**, *18*, 1015.
[10] M. George, T. E. Abraham, *J. Controlled Release* **2006**, *114*, 1.
[11] G. Helenius, H. Bäckdahl, A. Bodin, U. Nannmark, P. Gatenholm, B. Risberg, *J. Biomed. Mater. Res. A* **2006**, *76*, 431.
[12] N. Yamada, T. Okano, H. Sakai, F. Karikusa, Y. Sawasaki, Y. Sakurai, *Macromol. Rapid Commun.* **1990**, *11*, 571.
[13] R. Landers, A. Pfister, U. Hübner, R. John, R. Schmelzeisen, R. Mülhaupt, *J. Mater. Sci.* **2002**, *37*, 3107.
[14] A. Hoffman, *Adv. Drug Delivery Rev.* **2002**, *54*, 3.
[15] S. Naik, J. Pittman, J. Richardson, *J. Rheol.* **1976**, *20*, 639.
[16] R. Censi, P. Di Martino, T. Vermonden, W. E. Hennink, *J. Controlled Release* **2012**, *161*, 680.
[17] Y. C. Huang, C. Simmons, D. Kaigler, K. G. Rice, D. J. Mooney, *Gene Ther.* **2005**, *12*, 418.
[18] J. E. Phillips, K. L. Burns, J. M. Le Doux, R. E. Guldberg, A. J. García, *Proc. Natl. Acad. Sci. USA* **2008**, *105*, 12170.
[19] R. W. Carthew, E. J. Sontheimer, *Cell* **2009**, *136*, 642.
[20] M. Ø. Andersen, P. Dillschneider, J. Kjems, *RNA Interference from Biology to Therapeutics* (Ed: K. A. Howard), Springer, Heidelberg **2012**, 57.
[21] M. Ø. Andersen, J. Kjems, *Active Implants and Scaffolds for Tissue Regeneration* (Ed: M. Zilberman), Springer, Heidelberg **2011**, 145.
[22] W. C. Low, P. O. Rujitanaroj, D. K. Lee, P. B. Messersmith, L. W. Stanton, E. Goh, S. Y. Chew, *Biomaterials* **2013**, *34*, 3581.
[23] M. Monaghan, A. Pandit, *Adv. Drug Delivery Rev.* **2011**, *63*, 197.
[24] J. Zoldan, A. K. Lytton-Jean, E. D. Karagiannis, K. Deiorio-Haggar, L. M. Bellan, R. Langer, D. G. Anderson, *Biomaterials* **2011**, *32*, 7793.
[25] B. Levi, J. S. Hyun, E. R. Nelson, S. Li, D. T. Montoro, D. C. Wan, F. J. Jia, J. C. Glotzbach, A. W. James, M. Lee, M. Huang, N. Quarto, G. C. Gurtner, J. C. Wu, M. T. Longaker, *Stem Cells* **2011**, *29*, 2018.
[26] K. Wu, W. Song, L. Zhao, M. Liu, J. Yan, M. Ø. Andersen, J. Kjems, S. Gao, Y. Zhang, *ACS Appl. Mater. Interfaces* **2013**, *5*, 2733.
[27] M. Ø. Andersen, K. A. Howard, S. R. Paludan, F. Besenbacher, J. Kjems, *Biomaterials* **2008**, *29*, 506.
[28] T. Xu, K. W. Binder, M. Z. Albanna, D. Dice, W. Zhao, J. J. Yoo, A. Atala, *Biofabrication* **2012**, *5*, 015001.
[29] W. Schuurman, V. Khristov, M. W. Pot, P. R. van Weeren, W. J. A. Dhert, J. Malda, *Biofabrication* **2011**, *3*, 021001.
[30] J. Y. Wong, A. Velasco, P. Rajagopalan, Q. Pham, *Langmuir* **2003**, *19*, 1908e13.
[31] D. W. Hutmacher, *Biomaterials* **2000**, *21*, 2529.
[32] D. W. Hutmacher, R. E. Horch, D. Loessner, S. Rizzi, S. Sieh, J. C. Reichert, J. A. Clements, J. P. Beier, A. Arkudas, O. Bleiziffer, U. Kneser, *J. Cell. Mol. Med.* **2009**, *13*, 1417.
[33] D. W. Hutmacher, *J. Biomater. Sci., Polym. Ed.* **2001**, *12*, 107.
[34] A. Nelson, M. Gao, T. Boland, *Report on 2009 Biomaterials Day at Clemson University* (Ed: J. Nagatomi), Clemson University, Clemson, SC, USA **2009**, 23.
[35] S. J. Song, J. Choi, Y. D. Park, S. Hong, J. J. Lee, C. B. Ahn, H. Choi, K. Sun, *Artif. Organs* **2011**, *35*, 1132.
[36] P. S. Maher, R. P. Keath, K. Donnelly, R. E. Mackay, J. Z. Paxton, *Rapid Prototyping J.* **2009**, *15*, 204.
[37] T. Xu, J. Rohozinski, W. Zhao, E. C. Moorefield, A. Atala, J. J. Yoo, *Tissue Eng. Part A* **2009**, *15*, 95.
[38] V. Mironov, V. Kasyanov, C. Drake, R. R. Markwald, *Regener. Med.* **2008**, *3*, 93.
[39] Z. Bengali, A. K. Pannier, T. Segura, B. C. Anderson, J.-H. Jang, T. A. Mustoe, L. D. Shea, *Biotechnol. Bioeng.* **2005**, *90*, 290.
[40] C. S. Fjeldbo, K. Misund, C. C. Günther, M. Langaas, T. S. Steigedal, L. Thommesen, A. Laegreid, T. Bruland, *Methods Mol. Biol.* **2010**, *629*, 175.
[41] J. L. Simonsen, C. Rosada, N. Serakinci, J. Justesen, K. Stenderup, S. I. Rattan, T. G. Jensen, M. Kassem, *Nat. Biotechnol.* **2002**, *20*, 592.
[42] J. F. Bentzon, K. Stenderup, F. D. Hansen, H. D. Schroder, B. M. Abdallah, T. G. Jensen, M. Kassem, *Biochem. Biophys. Res. Commun.* **2005**, *330*, 633.